COMPUTATION OF UNSTEADY FLOWFIELD AND INDUCED NOISE FOR FLOW PAST A 3D WING WITH FLAPS IN LANDING CONFIGURATION

Amit Thakur, Prashant Rai, Felix Mudiappan, Sourabh Jain
Zeus Numerix Private Limited, Mumbai, India

Guillaume Alleon
EADS Innovation Works, Singapore

ABSTRACT

A coupled CFD-CAA tool is used to predict noise from a 3-D high lift wing with two flaps in landing configuration. Unsteady RANS CFD solver is used to predict the flow field, differential Ffowks Williams and Hawkings (FWH) equation is used to compute noise sources due to fluctuations in the flow, Boundary Element Method (BEM) based CAA solver is used to predict sound wave propagation in farfield. The directivity pattern of Sound Pressure Level (SPL) at dominant frequency shows rather uniform noise distribution in all directions, with peak noise being 66 dB @ 25 C_{root} from the wing.

INTRODUCTION

Aircraft takeoff and landing noise is increasing becoming an important area of concern to be addressed at the design stage. Engines, high lift wings and landing gear are the main sources of aerodynamic noise. With the advent of high bypass ratio turbofan engines, engine noise has reduced considerably; hence airframe noise is comparable to engine noise during landing. Numerical simulation, involving a coupled unsteady CFD simulation of flow in near-field and CAA (Computational Aero-Acoustics) simulation of sound wave propagation in farfield, is an important tool for predicting airframe noise of various design configurations.

CFD has been widely used in predicting high lift wing aerodynamics[1]. However, most of the studies are limited to computationally easier 2-D steady simulations. As expected, these simulations deviate from experiments when 3-D effects become prominent at higher angle of attack. 3-D steady simulations of multi-element high lift wings have also been performed. The grid size for structured grid was ~ 1.5 - 5 mn in most cases, though it even exceeded 10 mn in a few cases where geometric details such as brackets were included. Boundary layer transition and turbulence modeling have a prominent influence on the accuracy of simulations. Many experiments trip the wing boundary layer to achieve turbulence, modeling of this transition in CFD is important to accurately capture the flow field. Spalart Allmaras turbulence model is widely used as the model of

choice in simulations, it performs well even for separated flow at higher angle of attack. Running unsteady simulations on large grids is computationally expensive, hence 3-D unsteady simulations are extremely rare. However, such simulations are necessary for aeroacoustics since unsteadiness in the flow field is the source of noise.

At high slat/flap deflection angle and/or high angle of attack, a high lift wing may have several local regions of unsteady flow field. The slat cove (gap between slat and main airfoil) and flap cove (gap between main airfoil and flap) have separated flow containing eddies in a recirculation region[2]. Some of these eddies escape through the gap and get stretched longitudinally by the accelerating main flow; these eddies also contribute to flow separation in their wake. Such detailed flow features can only be captured by high accuracy turbulence models such as LES/DES. At high flap deflection angle, flow separates and forms a recirculation vortex on the flap upper surface[2, 3, 4, 5]. If flap deflection is increased further, vortices may be shed in the flap wake. Flap side edge vortex is a prominent source of flow unsteadiness and hence contributes to noise[6, 7, 8, 9, 10]. As flap deflection angle is increased, the pressure difference between high pressure flap lower surface and low pressure flap upper surface increases. At flap side edge, this pressure gradient pushes the flow from flap lower surface to flap upper surface. This turning flow rolls up along the flow direction and forms a tip vortex originating at the flap side edge, much like the wing tip vortex at high angle of attack. Tip fences mounted at the flap side edge weaken the vortex by preventing turning of flow along the side edge[11].

The purpose of present work is to estimate far-field noise for a 3D wing with two flaps configuration during aircraft landing. Unsteady RANS CFD solver is used to compute flow field around the wing. The acoustic noise sources in the form of monopoles and dipoles are calculated using differential FWH formulation on a control surface that encloses most of the quadrupole noise sources. The noise sources thus computed are then provided to BEM based CAA solver which computes noise at a point in the acoustic farfield.

GRID AND SOLVER SETUP

The 3D grid for flow past wing with two flaps was made using GridZ™. Grid independence study was performed to obtain a minimum grid size that still gives accurate aerodynamic coefficients. Steady state simulations were performed for grid independence study.

The surface grid size was minimized for the flap-stowed configuration. A 3.85 mn grid with 45,282 surface grid cells was the base grid. The surface grid cells were reduced along the chord and span to 25,298; the volume grid reduced to 2.22 mn. Since flow past a wing has sharper gradients along the chord than the span, the surface grid cells were reduced less liberally along the chord than the span. As shown in Table 1, compared to 3.85 mn grid, 2.22 mn grid simulation results had up to ~ 2% change in aerodynamic coefficients.

The volume grid was optimized for flap-deployed configuration. Keeping the same parameters as the 2.22 mn flap-stowed configuration grid, the flap-deployed configuration grid had 2.39 mn cells. The number of cells

were progressively reduced on all sides of the wing (ahead, above, behind, below and side) to get 1.78 mn and 1.33 mn grid. The aerodynamic coefficients obtained by running simulations on various grids are shown in Table 2. Compared to 2.39 mn grid, 1.78 mn grid had negligible change in C_L and C_D; for 1.33 mn grid, the variation was ~ 2%. With 1.33 mn grid as the base grid, clustering near the walls was substantially increased to capture the boundary layer without using wall function. The number of cells were increased to compensate for the sparse grid density away from the wall due to clustering. The first cell distance y^+ was within 3, the number of cells were 2.9 mn; unsteady simulations were run on this grid. The grid is for the configuration where flap translation is 0.66 m in horizontal direction and 0.01 m in vertical direction, flap deflection angle is 40^0 (for both flaps).

The surface grid is shown in Figure 1, the swept wing configuration and two partial-span flaps are visible. The grid is clustered at the main airfoil and flap leading and trailing edges, main airfoil tip and flap side edge. The topology of volume grid is shown in Figure 2. The grid has C-topology along the chord and H-topology along the span. The domain dimensions are C, $3C$, $3.2C$ and $2.9C$ ahead, above, behind and below the wing surface respectively (C = 6.1 m, chord @ main airfoil root) and $0.3S$ on the side from main airfoil tip (S = 15.5 m, main airfoil span). No-slip wall boundary condition is assigned to the wing surface, the plane along the main airfoil root is assigned inviscid wall, all other grid boundaries are assigned as far-field. Cross-sections of the grid at $0.06S$ and $0.93S$ from main airfoil root are shown in Figures 3 and 4 respectively; a closeup of the grid at $0.06S$ from root is shown in Figure 5. The grid has high clustering near the main airfoil and flap walls to capture the boundary layer. The grid has high cell density in the flap near-field to capture its unsteady wake. The cove between main airfoil and flap has high cell density to capture the flow field in this region. Grid distribution at the flap side edge and at main airfoil tip are shown in Figures 6 and 7 respectively. These regions have moderate cell density to capture the tip vortices that may be formed at medium/high angle of attack.

A finite volume, density based, unsteady RANS CFD solver FlowZ™ was used for simulation of flow past the wing. Implicit LUSGS (Lower Upper Symmetric Gauss Siedel) scheme with dual time stepping was used to achieve time accuracy for unsteady flows. Dual time stepping involves an inner iteration loop with pseudo time step and an outer update with physical time step. FlowZ™ was run with freestream M = 0.3 and angle of attack α = 7^0. Spalart Allmaras model was used for turbulence simulation. The physical time step was 0.1 ms with 10 sub-iterations per time step. The numerical scheme employed was HLLC. The gradient calculations were done using Green's theorem. Simulations were performed in parallel environment utilizing 12 CPUs @ 2.2 GHz and 12 GB RAM. As expected, unsteady 3-D wing flowfield simulation was computationally demanding and needed 1-2 weeks for a simulation.

COMPUTATIONAL AERO-ACOUSTICS

The theoretical basis for calculating noise sources is based on the Ffowks Williams and Hawkings (FWH) method; the differential formulation is shown below.

$$(\frac{1}{c_0^2}\frac{\partial}{\partial t^2}-\frac{\partial}{\partial x_i^2})[Hc_0^2(\rho-\rho_0)]=\frac{\partial}{\partial t}[\rho_0 U_n|\nabla f|\delta(f)]-\frac{\partial}{\partial x_i}[L_i|\nabla f|\delta(f)]+\frac{\partial^2}{\partial x_i \partial x_j}[HT_{ij}]$$

$$L_i=[\rho u_i u_j+(p-p_0)\delta_{ij}]n_j$$

$$U_n=U_i n_i$$

$$U_i=\frac{\rho u_i}{\rho_0}$$

The control surface *f* is defined as follows.

f = 0 (on the control surface)

f > 0 (within the fluid field)

f < 0 (elsewhere)

The Heavyside function *H* is defined as follows.

H (*f*) = 1 for *f* > 0

H (*f*) = 0 for *f* < 0

The left hand side of the differential equation is a wave equation representing the propagation of noise, and the right hand side represents the sources of noise generated due to the unsteady flow field. The CFD-CAA coupling code computes the noise sources from unsteady flow parameters obtained from CFD. It is input to CAA solver Actipole which computes the propagation of noise in the farfield.

The 1st term on right hand side represents the monopole noise sources, the 2nd term represents the dipole sources, the 3rd term represents the quadrupole sources. It can be seen mathematically from the equation that the monopole and dipole sources are defined only on the control surface *f*, the quadrupole sources are defined in the volume outside the control surface *f*. FWH method has the flexibility of selecting the control surface *f* anywhere in the fluid flow domain, and not just the solid surface of a body. This can be cleverly utilized by selecting *f* such that it encloses most of the quadrupole noise sources. In that case, only the surface computations of monopole and dipole sources need to be performed and volume computations of quadrupole sources can be neglected, without sacrificing computational accuracy. Hence the 3rd term on right hand side of FWH differential equation can be neglected for a suitably chosen control surface.

The monopole and dipole noise source terms on the right hand side of FWH differential equation have the unit of source strength per unit area. It needs to be multiplied by control surface element area *dS* to get the point noise source strength for input to Actipole. The term $|\nabla f|$, representing the magnitude of surface element normal, is not explicitly included in the monopole and dipole expressions, since it is now a part of surface element area *dS*.

$$M=\frac{\partial}{\partial t}\left[\rho_0 U_n \delta(f)\right]*dS$$

$$D = -\frac{\partial}{\partial x_i}\left[L_i\,\delta(f)\right] * dS$$

$$dS = |\nabla f| * dA$$

For dipole, in addition to the source strength, Actipole also takes the direction vector as an input. It places two monopoles of equal and opposite strengths along the direction vector. In the coupling code, the dipole strength is resolved along the three coordinate axes as follows.

$$D_x = -\frac{\partial}{\partial x}\left[L_1\,\delta(f)\right] * dS$$

$$D_y = -\frac{\partial}{\partial y}\left[L_2\,\delta(f)\right] * dS$$

$$D_z = -\frac{\partial}{\partial z}\left[L_3\,\delta(f)\right] * dS$$

D_x, D_y, D_z have direction vectors (1, 0, 0), (0, 1, 0), (0, 0, 1) respectively.

Unsteady RANS CFD simulation is run using the implicit version of FlowZ™. The monopole and dipole noise source computation on the control surface *f*, using the FWH formulation described above, are performed in FlowZ™ at discrete time steps. Separate files are generated for each noise source type, 1 for monopole and 3 for dipole (components about the 3 axes).

A Fourier transformation code to convert flow-field data of a given variable in time domain into frequency domain data was developed. Using this code, the monopole and dipole source data in time domain are converted into frequency domain data. In addition to noise sources, Actipole also needs the surface mesh of the body as input to account for sound wave reflection from walls. The solver implements Boundary Element Method (BEM) to find the solution of wave equation in a 3-D homogeneous medium.

CFD RESULTS

The eddy viscosity contours at various cross-sections along the wing span and at t = 0.38 sec are shown in Figures 8 - 12. The cross-sections in Figures 8 and 9 are along flap-1, the cross-section in Figure 10 is near the junction between flap-1 and flap-2, the cross-sections in Figures 11 and 12 are along flap-2. Due to high flap deflection angle (40^0), boundary layer separates on the flap upper surface and forms a recirculation vortex. A recirculation bubble is also formed in the flap cove region. A free shear layer is formed at the flap trailing edge. The main airfoil boundary layer gets thicker along the span from root to tip, infact there is a localized region of flow separation and a recirculation bubble on the main airfoil upper surface (Figures 10, 11). This is probably due

to lower Reynolds number flow in smaller chord regions of the wing, such flow has less inertia to withstand adverse pressure gradients. A thicker / separated boundary layer on the main airfoil increases inflow turbulence on the flap and hence causes larger flow separation on the flap upper surface (Figure 11). The streamlines around the wing tip and flap side edge are shown in Figures 13 and 14 respectively. A moderate wing tip vortex is formed at 7^0 angle of attack. However, no tip vortex is seen at the flap side edge even for 40^0 flap deflection angle.

CAA RESULTS

A validation simulation was performed for flow past a 2-D cylinder at $M = 0.6$, $Re = 1000$[12]. The results, shown in Table 3, are compared with reference experimental and CFD-CAA data in literature[13]. The primary source of noise are the periodic vortices shed in the cylinder wake. The Sound Pressure Level (SPL) in reference experiment at $r = 128D, \theta = 90^0$ is 98 dB. The reference CFD-CAA result for 3-D geometry (101 dB) is more accurate than that for 2-D geometry (116 dB). In the present 2-D simulation, the dipole noise components are 106 and 109 dB; monopole noise is negligible (57 dB).

For the wing simulation, an elliptical FWH control surface shown in Figure 15 is defined to compute the monopole and dipole noise sources.

$$\frac{(x-x_0)^2}{a^2}+\frac{(y-y_0)^2}{b^2}=1$$

$a = 6.5$, $b = 2.1$, $x_0 = 0$, $y_0 = 0.1$ (m)

The major/minor axes and origin of the ellipse is chosen to enclose the swept wing along its chord and the flap wake; the length of the ellipse encloses the wing span and the wing tip wake. The control surface is an open surface, this is not a constraint in the FWH formulation. The coupling code discretizes the elliptical surface modeled by the equation into several points, and searches for the CFD mesh cell centres closest to these points to construct the approximate control surface. The CFD mesh cell sizes are coarse away from the wall, hence the control surface created in this region is not smooth. This feature does not affect the accuracy of CAA simulations since Actipole reads the noise sources on a set of random data points rather than points on a well defined surface.

After transients in unsteady CFD simulation had subsided, noise sources were sampled every 0.1 ms and for 0.18 s duration; it corresponds to frequency spectrum in the range 5.5 – 5000 Hz. The frequency spectrum for dipole noise sources at a point on the control surface 90^0 from + x axis, $z / S = 0.7$ is shown in Figure 16, monopole noise sources are negligible. The noise sources are contained in the frequency range < 1000 Hz. The oscillation of vortex on the flap upper side may contribute a low frequency peak to the spectrum; a movie created

from unsteady CFD data estimates the frequency as < 100 Hz. The multiple broadband peaks observed in the spectrum may be attributed to the eddies in the flap trailing edge shear layer, and to a lesser extent the weak wing tip vortex. The dominant peak is observed at f = 128 Hz, the farfield noise simulation is performed at this frequency.

The requirement of surface mesh input to a BEM based CAA solver is quite different from the mesh input to a CFD solver due to different physics being solved. The CAA solver needs a uniform surface mesh with approximately $\lambda/10$ cell size. For bigger wavelengths, the cell size can be smaller, especially for surfaces with curvature to adequately capture the geometry. A wing surface mesh different from the CFD mesh was created; the average cell size is $\lambda/24$ (f = 128 Hz / λ = 2.7 m).

The directivity plot of dipole Sound Pressure Level (*dB*) at $r = 25\ C_{root}$, z = 0 (wing root) for f = 128 Hz is shown in Figure 17. The flow direction is shown in the figure. As expected, dipole noise component along z-axis (span) is negligible compared to x and y axis components, which have similar contribution to total dipole noise. Again as expected, dipole x and y components show higher noise levels along their axes of orientation. Curiously, dipole component along x-axis shows more noise ahead of the wing than behind the wing. The total dipole noise distribution is rather uniform in all directions, peak noise level is 66 *dB*. It is noted that flap side edge vortex, a prominent source of noise at high flap deflection angle, was not observed in CFD simulation even at $\delta_{flap} = 40^0$; the noise level would be higher by a few *dB* if it was present in the flow.

CONCLUSION

Unsteady RANS CFD simulation of flow past a 3-D high lift wing with 2.9 mn grid cells was performed to capture noise sources using differential FWH formulation, BEM CAA solver was used to estimate farfield noise. RANS CFD is a less accurate, yet computationally less demanding tool appropriate for analyzing various wing configurations at the initial design stage. A more accurate aero-acoustic analysis of a finalized configuration can be performed with unsteady LES CFD simulation on a much finer mesh and smaller time steps; such an effort will require substantially more computational resources.

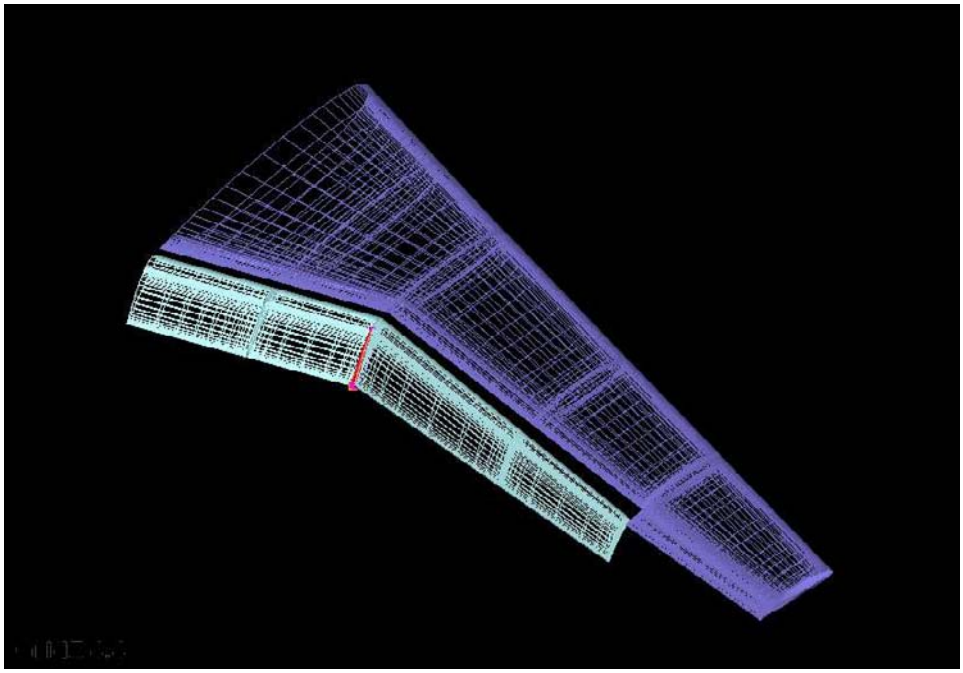

Figure 1. Surface grid of wing with flaps.

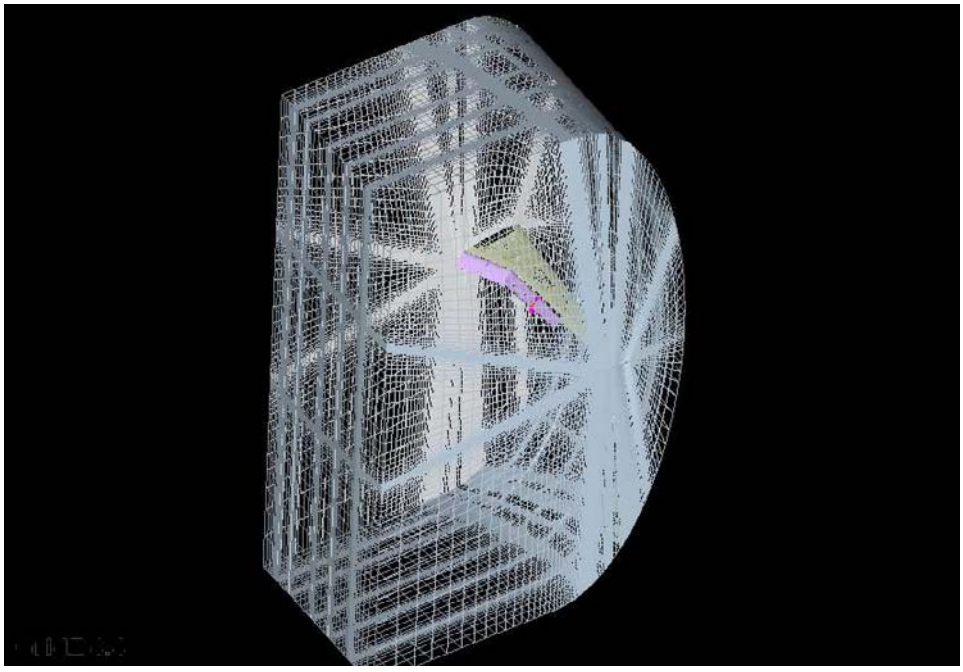

Figure 2. Topology of volume grid around wing with flaps.

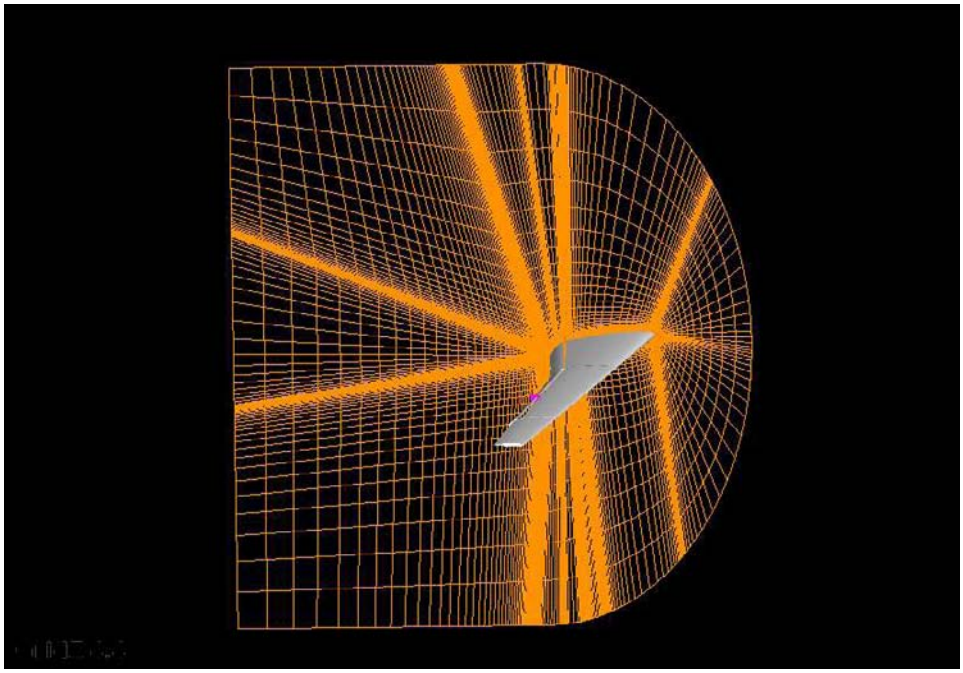

Figure 3. Grid cross-section @ 0.06*S* from root.

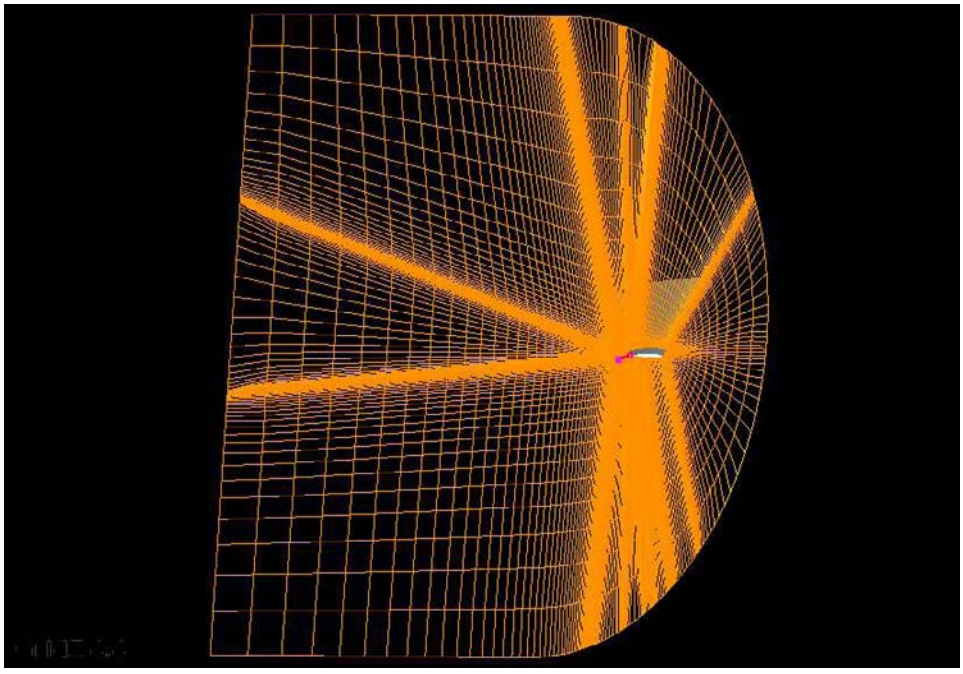

Figure 4. Grid cross-section @ 0.93*S* from root.

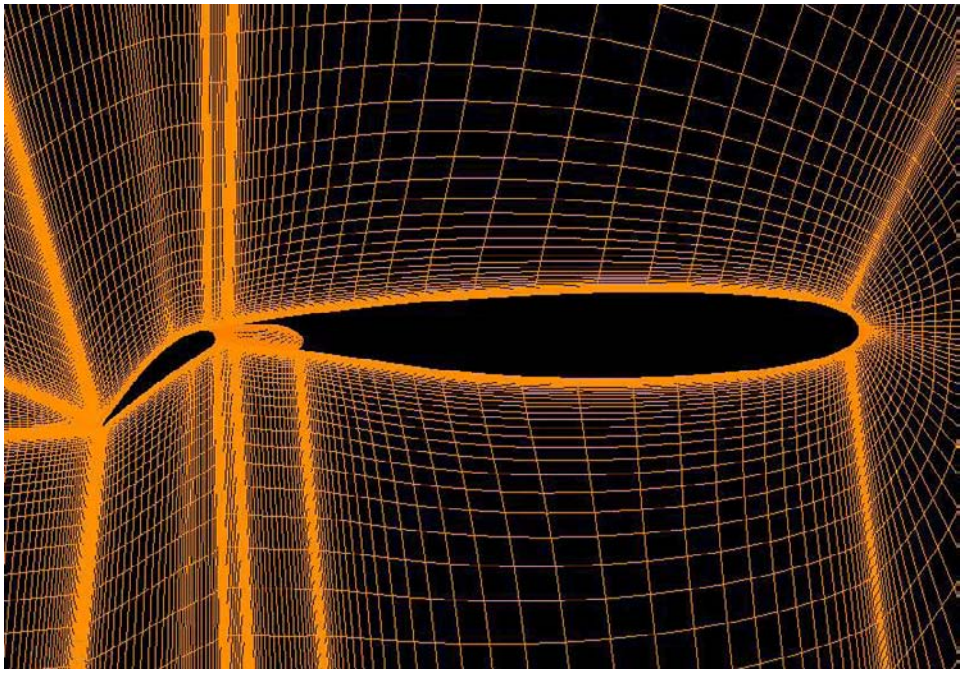

Figure 5. Closeup of grid cross-section @ 0.06*S* from root.

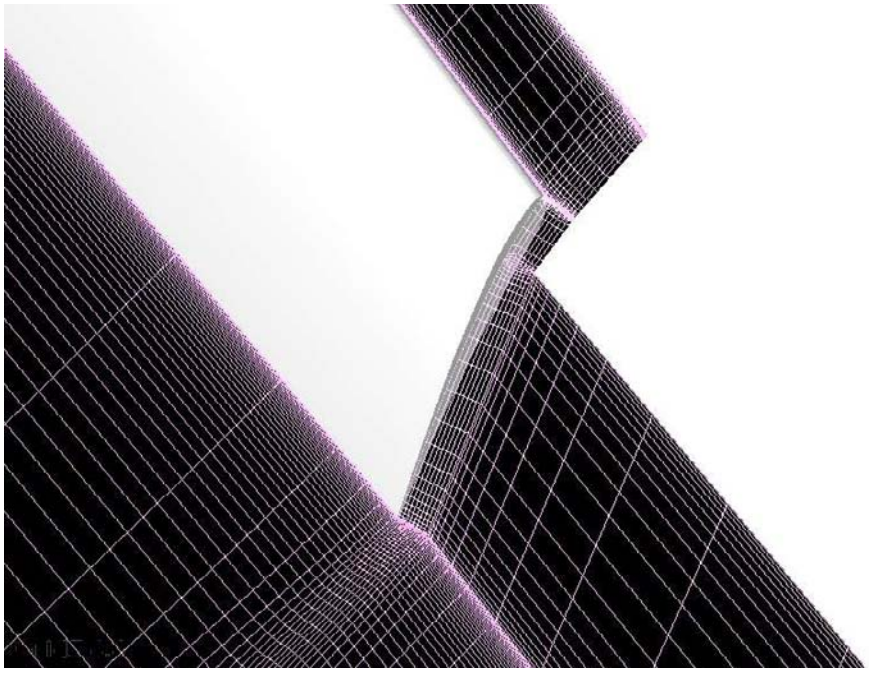

Figure 6. Grid distribution at the flap side edge.

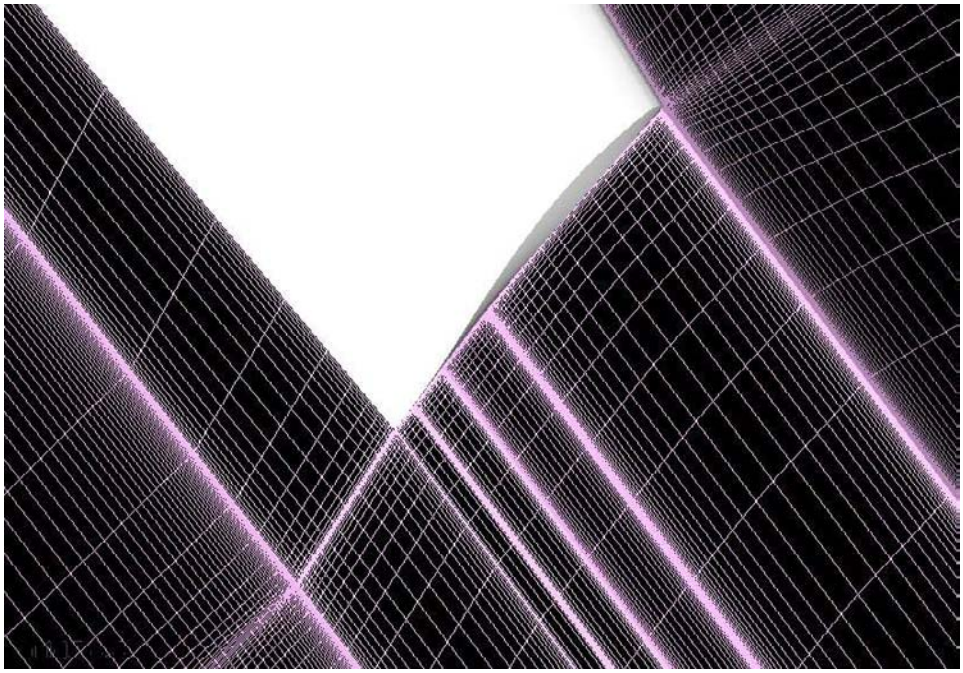

Figure 7. Grid distribution at the main airfoil tip.

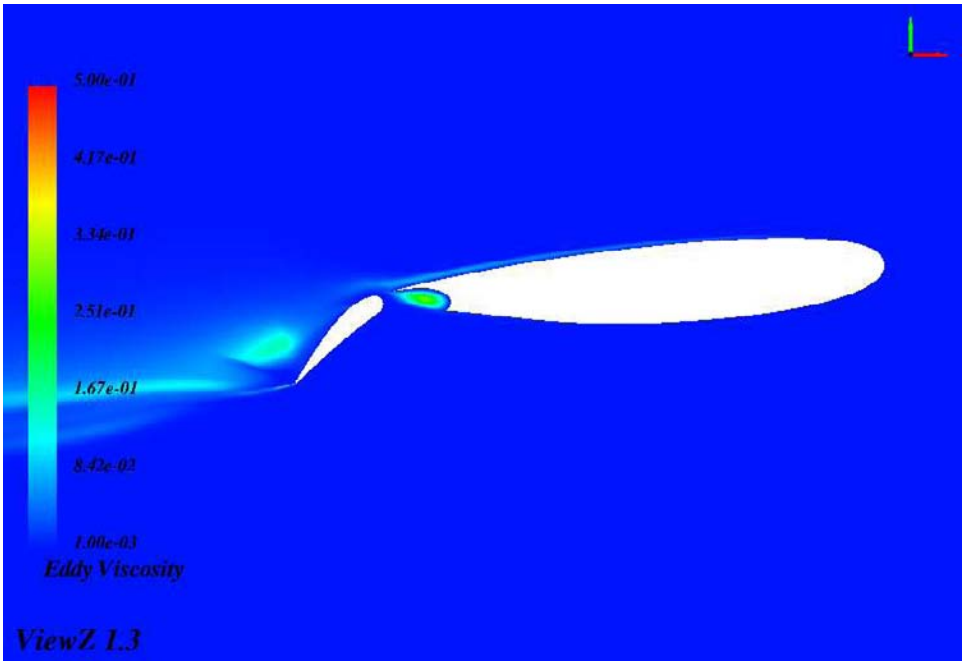

Figure 8. Eddy viscosity contours at 0.07S from the root.

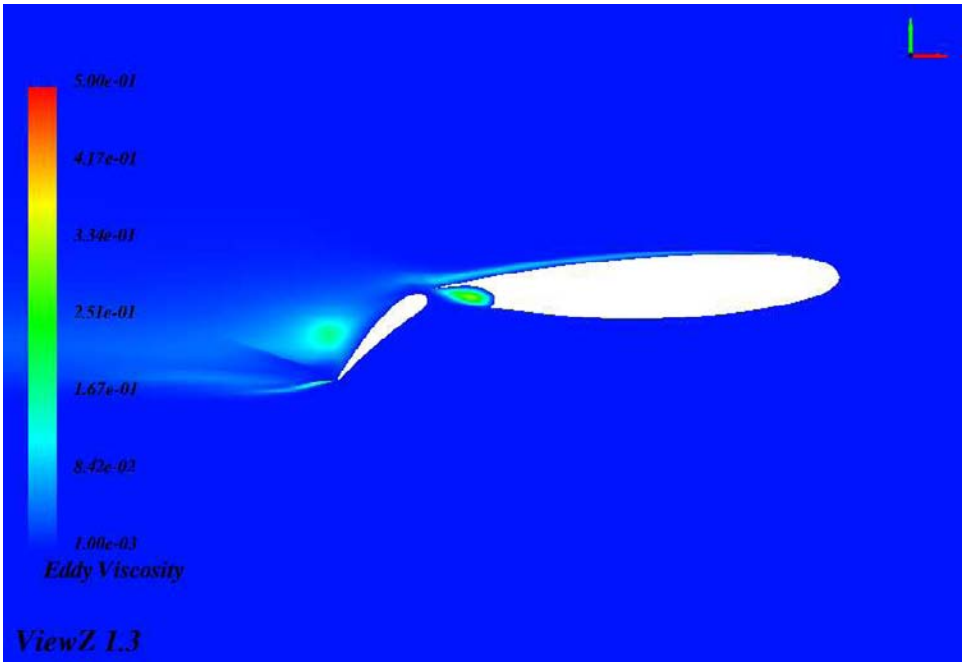

Figure 9. Eddy viscosity contours at 0.18S from the root.

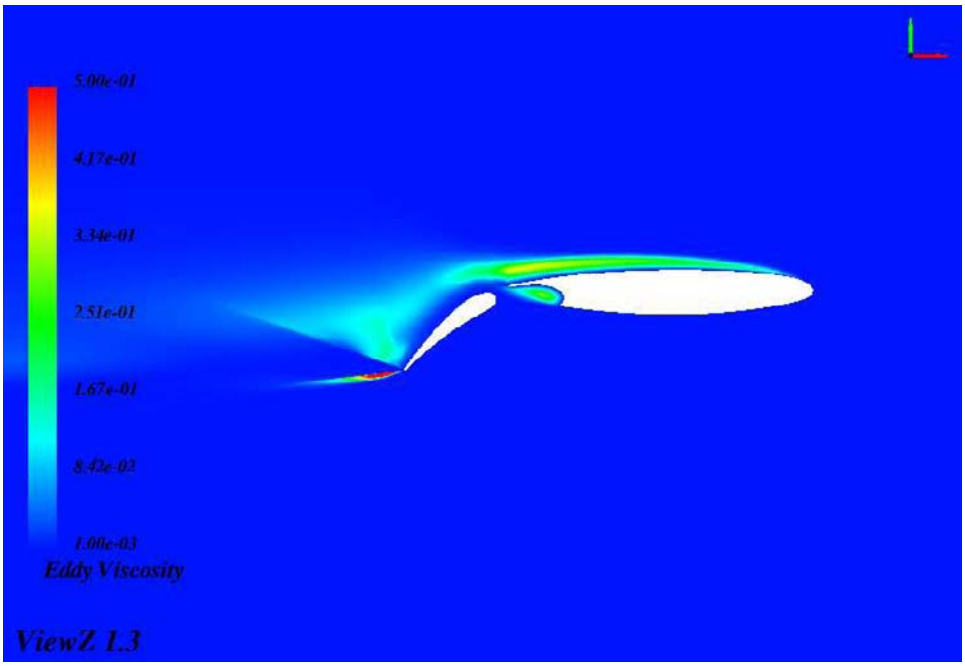

Figure 10. Eddy viscosity contours at 0.31S from the root.

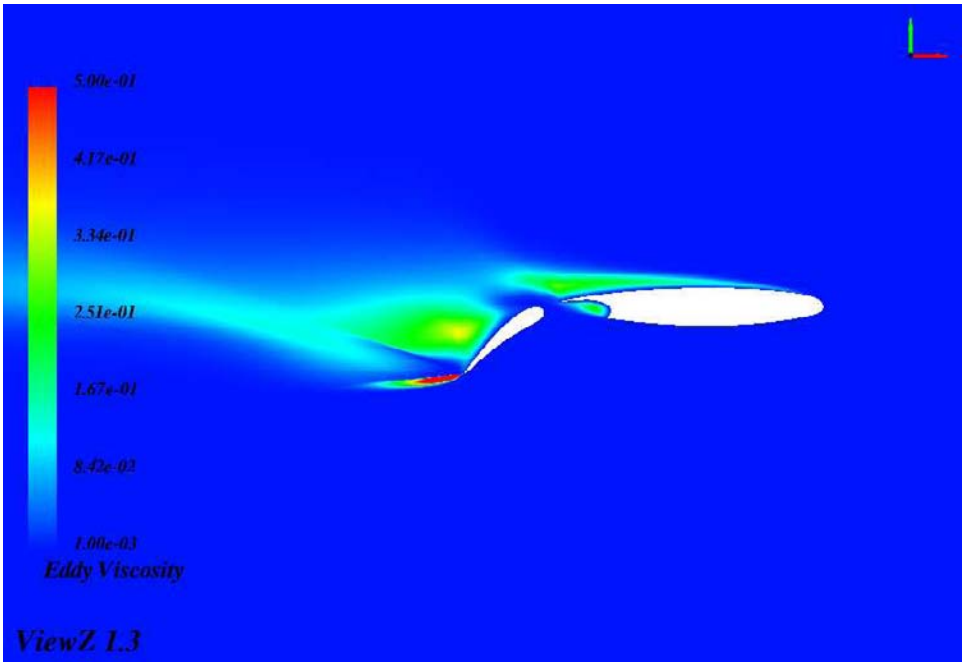

Figure 11. Eddy viscosity contours at 0.52S from the root.

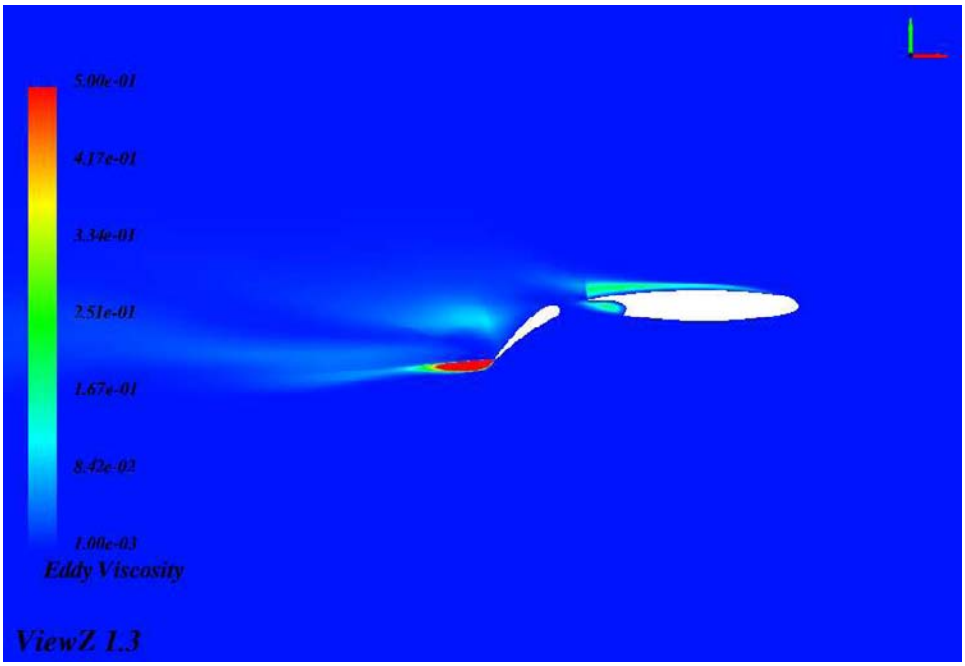

Figure 12. Eddy viscosity contours at 0.75S from the root.

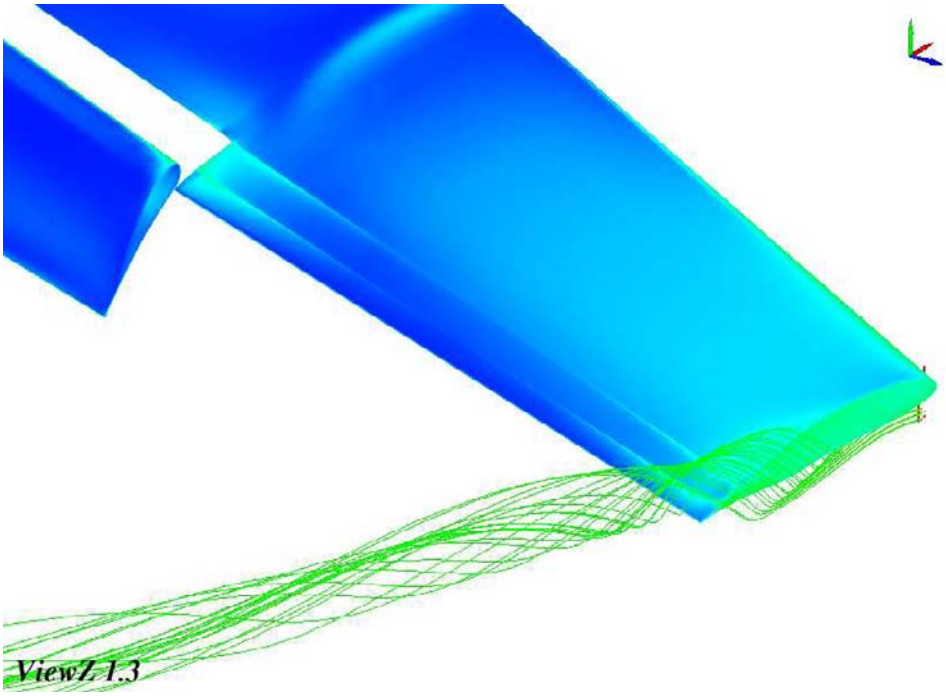

Figure 13. Flow streamlines at the wing tip.

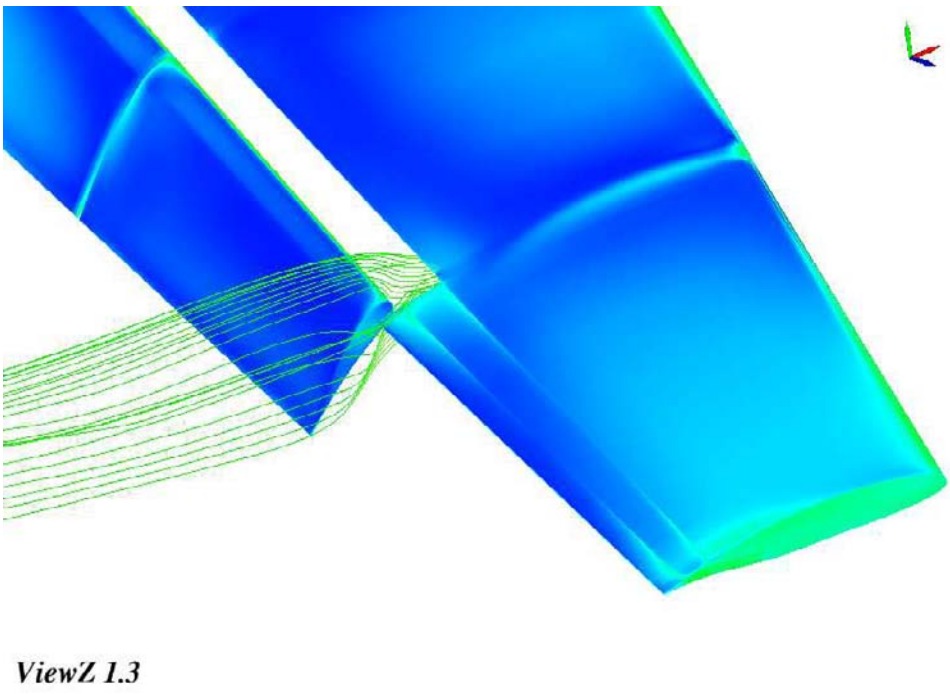

Figure 14. Flow streamlines at the flap side edge.

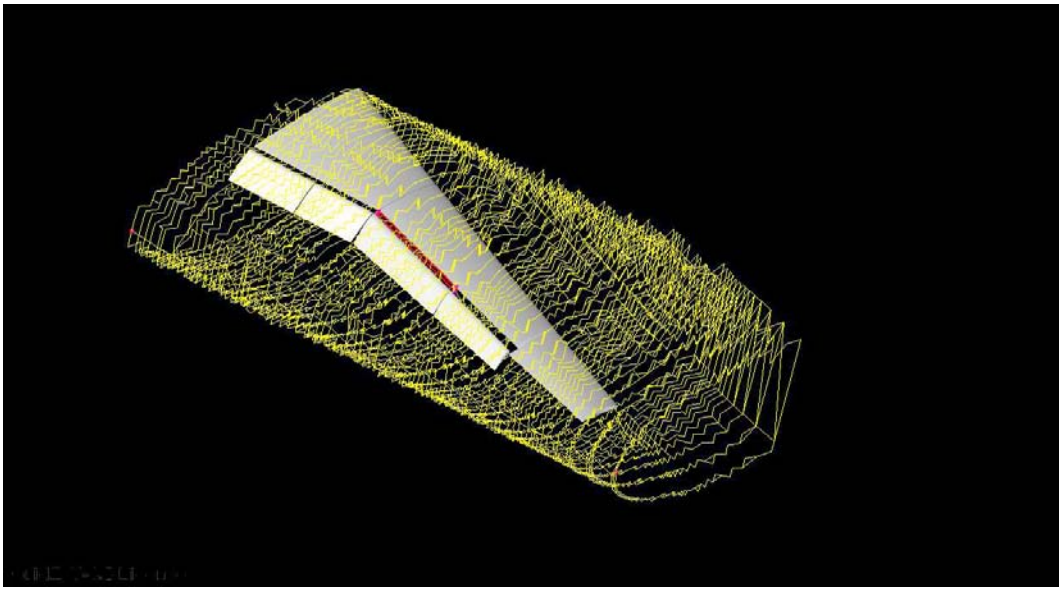

Figure 15. FWH control surface for noise sources computation.

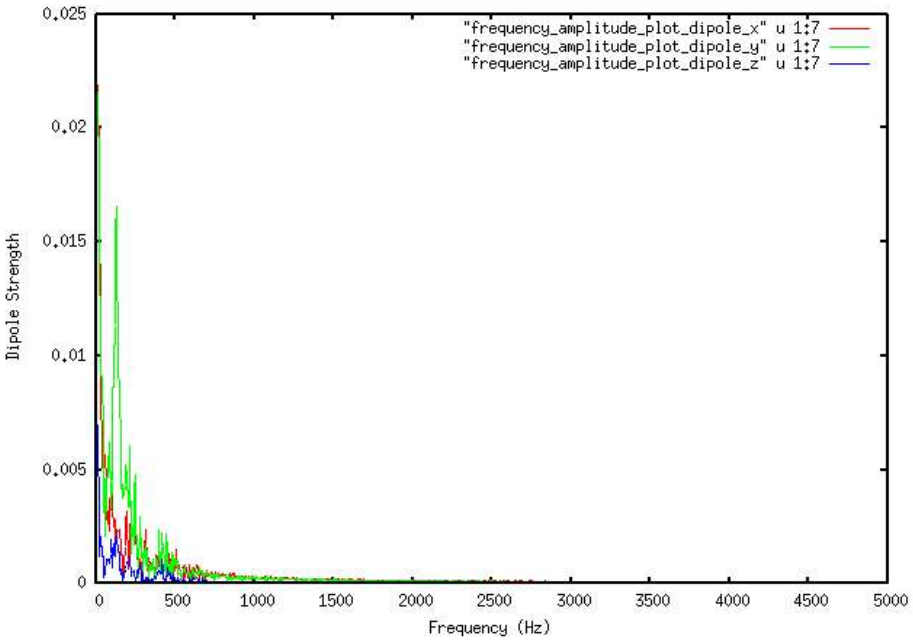

(a)

Figure 16. Frequency spectrum for dipole noise sources at a point on the control surface 90^0 from + x axis, z / S = 0.7.

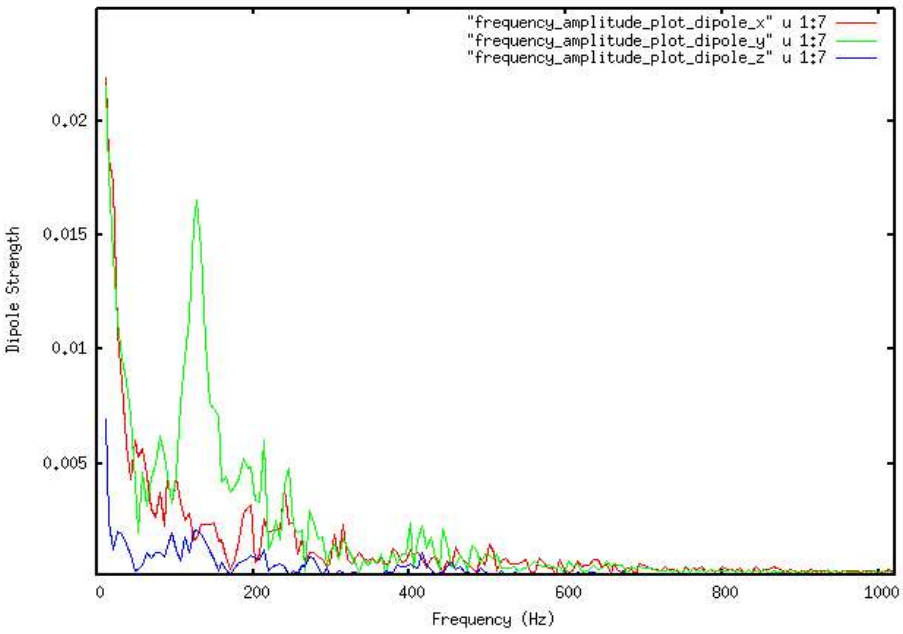

(b)

Figure 16. Continued.

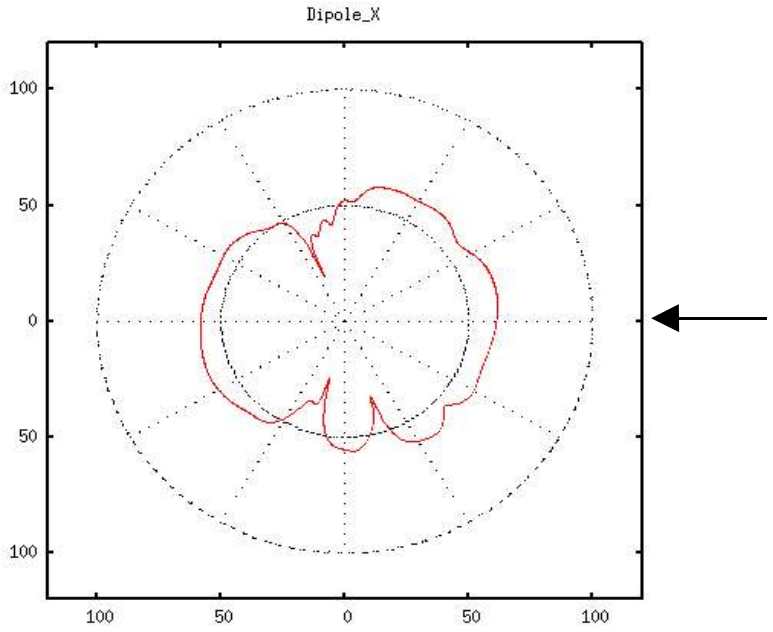

(a)

Figure 17. Directivity plot of dipole *SPL* (*dB*) at $r = 25\ C_{root}$, $z = 0$ for $f = 128$ Hz (a) dipole (*x*-axis) (b) dipole (*y*-axis) (c) dipole (*z*-axis) (d) dipole (total). The flow direction is indicated.

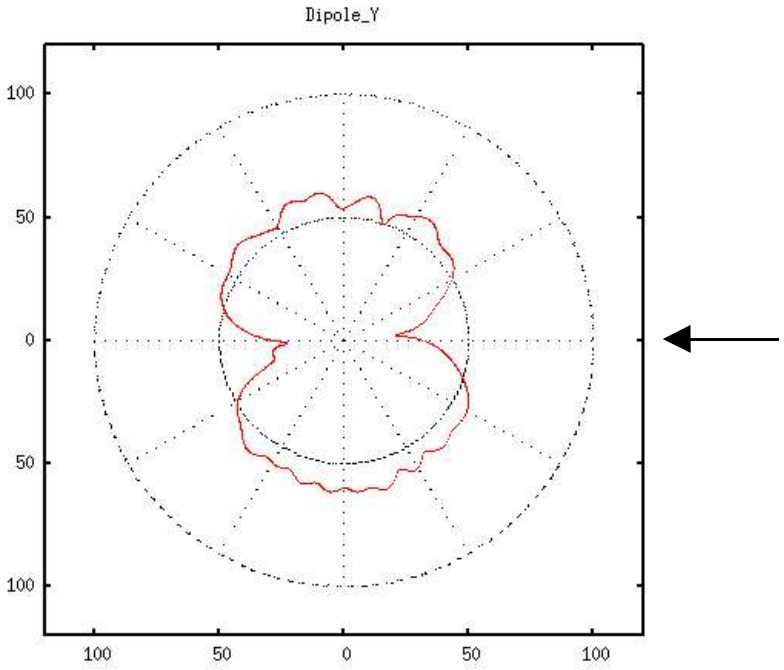

(b)

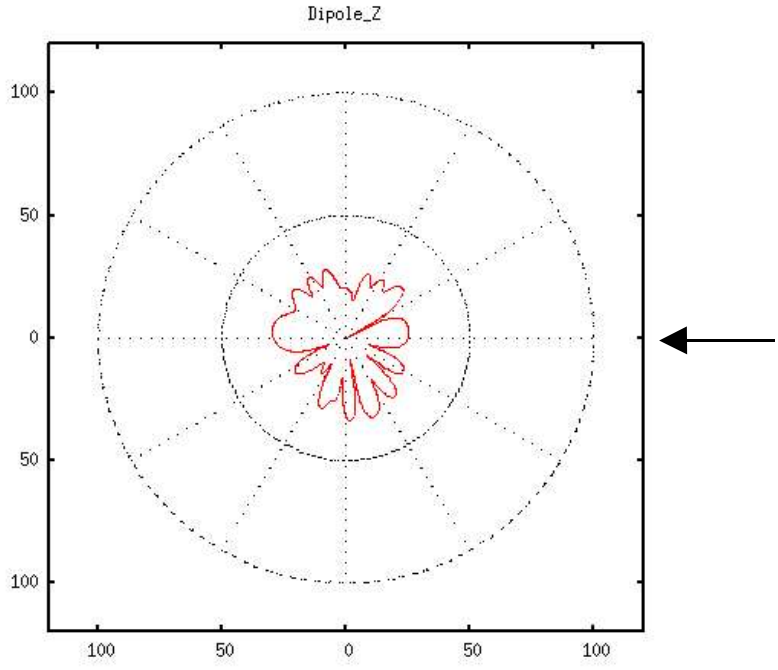

(c)

Figure 17. Continued.

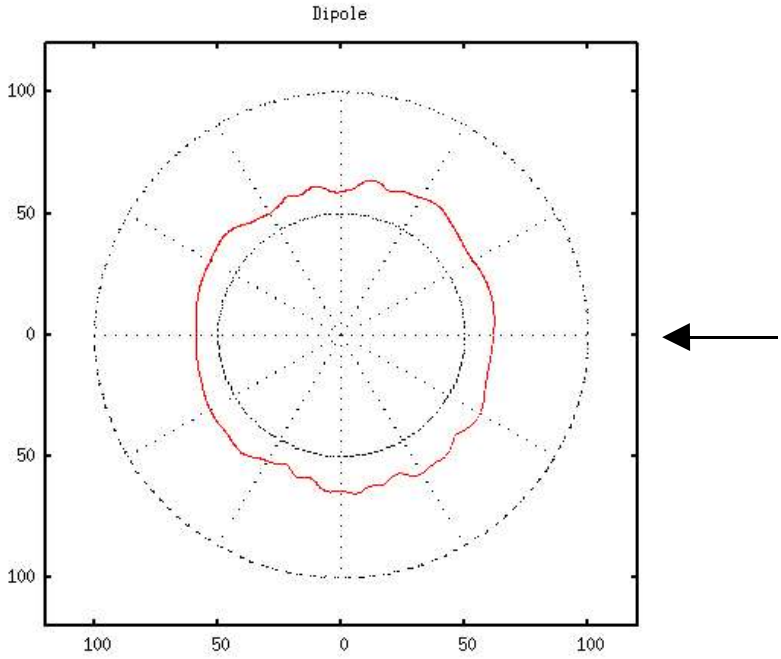

(d)

Figure 17. Continued.

Table 1. Grid independence study of surface grid.

Volume grid (million)	Surface grid	C_L (% difference)	C_D (% difference)
2.22	25298	0.7	-1.9
3.85	45282	0	0

Table 2. Grid independence study of volume grid.

Grid size (million)	C_L (% difference)	C_D (% difference)
1.33	2.1	1.8
1.78	0	0
2.39	0	0

Table 3. Comparison of *SPL* (dB) @ $r = 128D$, $\theta = 90^0$ from experimental results and CFL3D + WOPWOP.

	Experiment	CFL3D + WOPWOP	FlowZ™ + Actipole (Monopole)	FlowZ™ + Actipole (Lift Dipole)	FlowZ™ + Actipole (Drag Dipole)
SPL (dB)	98	116 (2-D), 101 (3-D)	57	106	109

REFERENCES

[1]Rumsey C. L. and Ying S. X., "Prediction of high lift: review of present CFD capability", *Progress in Aerospace Sciences*, 38, pp. 145-180, 2002.

[2]Deck S., "Zonal detached eddy simulation of the flow around a high lift configuration", *AIAA Journal*, 43 (11), pp. 2372-2384, 2005.

[3]Liu Yi., Sankar L. N., Englar R. J. and Ahuja K. K., "Numerical simulations of the steady and unsteady aerodynamic characteristics of a circulation control wing airfoil", *AIAA Paper*, AIAA-2001-0704, 2001.

[4]Carlson H. W. and Walkley K. B., "An aerodynamic analysis computer program and design notes for low speed wing flap systems", *NASA Contractor Report*, NASA CR 3675, 1983.

[5]Rudnik R., Melber S., Ronzheimer A. and Brodersen O., "Three dimensional Navier Stokes simulations for transport aircraft high lift configurations", *Journal of Aircraft*, 38 (5), pp. 895-903, 2001.

[6]Rumsey C. L., Biedron R. T. and Thomas J. L., "CFL3D: Its history and some recent applications", *NASA Technical Memorandum*, NASA TM 112861, 1997.

[7]Takallu M. A. and Laflin K. R., "Reynolds averaged Navier Stokes simulations of two partial span flap wing experiments", *AIAA Paper*, AIAA-1998-0701, 1998.

[8]Meadows K. R., Brooks T. F., Humphreys W. M., Hunter W. H. and Gerhold C. H., "Aeroacoustic measurements of a wing flap configuration", *AIAA Paper*, AIAA-1997-1595, 1997.

[9]Brooks T. F. and Humphreys W. M., "Flap edge aeroacoustic measurements and predictions", *Journal of Sound and Vibration*, 261, pp. 31-74, 2003.

[10]Guo Y. P., Joshi M. C., Bent P. H. and Yamamoto K. J., "Surface pressure fluctuations on aircraft flaps and their correlation with farfield noise", *Journal of Fluid Mechanics*, 415, pp. 175-202, 2000.

[11]Slooff J. W., De Wolf W. B., Vander Wal H. M. M. and Maseland J. E. J., "Aerodynamic and aeroacoustic effects of flap tip fences", *NLR Report*, NLR-TP-2002-004, 2002.

[12]Rai P, Thakur A and Alleon G, "Computation of vortex shedding and flow induced noise for a circular cylinder", *10th Annual CFD Symposium*, Bangalore India, P-39, 2008.

[13]Cox J. S., Brentner B. S. and Rumsey C. L., "Computation of vortex shedding and radiated sound for a circular cylinder", *Theoretical and Computational Fluid Dynamics*, 12, pp. 233-253, 1998.